Geomechanics and Engineering, *Vol. 18, No. 3 (2019) 235-245*
DOI: https://doi.org/10.12989/gae.2019.18.3.235

Face stability analysis of rock tunnels under water table using Hoek-Brown failure criterion

T.Z. Li* and X.L. Yang[a]

School of Civil Engineering, Central South University, Changsha, 410075, China

(Received January 8, 2019, Revised May 19, 2019, Accepted May 28, 2019)

Abstract. This paper presents a novel methodology for face stability assessment of rock tunnels under water table by combining the kinematical approach of limit analysis and numerical simulation. The tunnels considered in this paper are excavated in fractured rock masses characterized by the Hoek-Brown failure criterion. In terms of natural rock deposition, a more convincing case of depth-dependent m_i, GSI, D and σ_c is taken into account by proposing the horizontally layered discretization technique, which enables us to generate the failure surface of tunnel face point by point. The vertical distance between any two adjacent points is fixed, which is beneficial to deal with stability problems involving depth-dependent rock parameters. The pore water pressure is numerically computed by means of 3D steady-state flow analyses. Accordingly, the pore water pressure for each discretized point on the failure surface is obtained by interpolation. The parametric analysis is performed to show the influence of depth-dependent parameters of m_i, GSI, D, σ_c and the variation of water table elevation on tunnel face stability. Finally, several design charts for an undisturbed tunnel are presented for quick calculations of critical support pressures against face failure.

Keywords: face stability; pore water pressure; numerical simulation; horizontally layered discretization technique; Hoek-Brown failure criterion

1. Introduction

Face stability of tunnels under water table, such as cross-river tunnels, subsea tunnels or tunnels in water-rich areas, is greatly affected by pore water pressure especially for those driven in poor self-bearing capacity media (Ukritchon *et al.* 2017a, Hamrouni *et al.* 2018, Yang and Chen 2019). The commonly used methods for tunnel face stability assessment include limit analysis method (Mollon *et al.* 2010, 2011), limit equilibrium method (Perazzelli *et al.* 2014), finite element method (Sloan 201,; Ukritchon and Keawsawasvong 2017;, Ukritchon *et al.* 2017b) and so on. As for the pore water pressure, it is usually generated by seepage flow towards the tunnel when the hydrostatic head is higher than the piezometric head in front of tunnel face. In order to study the effect of seepage flow on tunnel face stability, the pore water pressure is usually treated as a constant external force applied on soil skeleton or rock masses. And several approaches for computing the pore water pressure were proposed in previous studies. Skempton (1954) defined the pore water pressure coefficients to characterize the pore pressure change in undrained soils. Accordingly, Bishop and Morgenstern (1960) suggested that the pore water pressure u could be calculated according to Eq. (1)

$$u = r_u \gamma h \tag{1}$$

where r_u represents the pore water pressure ratio; γ represents the unit weight of the overlying soils or rock masses and h represents the vertical distance measured from the specified point to the water table elevation. Michalowski (2002) introduced the coefficient r_u to calculate the pore pressure distribution in a uniform slope and presented the stability charts for practical use. Zhang and Yang (2019b) investigated the influence of water pressure on tunnel stability using limit analysis method. Instead of using r_u, Barros and Santos (2012) used a mathematical model to obtain the analytical solution for a steady-state seepage and calculated the active earth pressure on the possibly inclined face of a retaining wall. Similarly, Xu and Bezuijen (2018) proposed an analytical method to predict the excess pore water pressure in front of slurry shield in saturated sandy ground. Apart from previously mentioned researches, scholars also adopted numerical simulation approach to determine the pore water pressure. Lee *et al.* (2003) calculated the upper bound solution of the effective pressure retaining the tunnel face stability in which the seepage force was analyzed by numerical simulation approach under the condition of steady-state groundwater flow. Perazzelli *et al.* (2014) studied the tunnel face stability with seepage effects by proposing a limit equilibrium model. The steady-state hydraulic head field around the tunnel face was determined with the help of finite element programs.

It is a key problem to find a proper way to determine the water pressure distribution (Li and Yang 2018b), while

*Corresponding author, Ph.D. Student
E-mail: jacksonic@126.com
[a]Professor
E-mail: yangky@aliyun.com

ISSN: 2005-307X (Print), 2092-6219 (Online)

another important issue is how to incorporate the pore water pressure into the failure mechanism of tunnel face. Mollon *et al.* (2010, 2011) proposed an advanced two- and three-dimensional (2D and 3D) failure mechanism using the so-called spatial discretization technique which made it possible to join the discretized points into the steady-state flow net in the analysis. This approach is more convincing than the traditional ones in terms of the fact that the pore water pressure for each point can be determined respectively, not an average seepage pressure. Research results of this kind can be found in Pan and Dias (2016, 2018) where the hydraulic head induced by seepage flow was calculated using numerical method and interpolated for each discretized points ahead of tunnel face. Their findings give a new idea to explore the effects of pore water pressure on tunnel face stability. However, these studies are usually carried out with an assumption of uniform excavation media at the beginning which probably deviated from the actual situation. In reality, the properties of soils and rock masses are more likely depth-dependent from a geological perspective, which is lack of consideration in many researches.

Conventional opinions hold that the variation of the properties of rock masses is less obvious than that of soils, so few scholars have paid their attention to this issue (Li *et al.* 2019, Michalowski 2002, Ukritchon and Keawsawasvong 2018). In most studies, researches usually consider the uniform geomaterials when studying the stability of a tunnel in Hoek-Brown rock masses. Ukritchon and Keawsawasvong (2019a) combined the lower bound finite element limit analysis and semi-definite programming to investigate the stability of unlined square tunnels in Hoek-Brown material. Pan and Dias (2016) also treated the rock masses as uniform geomaterials in their studies in combination with numerical method. However, for a tunnel with a large cross section or whose failure domain extends relatively widely along the vertical direction, the variation of the properties of rock masses probably matters in the stability assessment. As a matter of fact, this issue has not been thoroughly investigated at present.

This paper is devoted to the face stability of a tunnel excavated in fractured Hoek-Brown rock masses considering the seepage flow conditions. Based on the kinematical approach of limit analysis, a novel horizontally layered discretization technique is presented to construct the 2D failure mechanism of tunnel face. The pore water pressure ahead of tunnel face is numerically determined using soft ware and interpolated for each discretized points. In the calculations, the parameters of m_i, GSI, D and σ_c vary with depth to respect the actual rock properties and different water table elevations are taken into account to calculate the critical support pressure against face failure. This combination of discretization-based failure mechanism and numerically obtained pore water pressure can give a better estimation of face stability of tunnels affected by depth-dependent rock parameters and pore water pressure.

2. Theoretical basis

2.1 Pore water pressure in the framework of limit analysis

Limit analysis method mainly consists of two theoretical foundations, namely the upper bound theorem (Michalowski 2002, Mollon *et al.* 2011, Luo and Yang 2018, Yang and Zhang 2018, Zhang *et al.* 2018, Zhang and Yang 2019a, Zhu and Yang 2018, Ukritchon and Keawsawasvong 2019b) and the lower bound theorem, both of which have been fully researched in existing works. Upper bound theorem of limit analysis has been considered as an effective tool to resolve the stability problems of geotechnical structures. In the framework of limit analysis, the pore water pressure is conventionally regarded as a part of external load applied on the kinematical admissible velocity field boundaries. This practice has been adopted by a larger number of scholars (Michalowski 2002). By incorporating the pore water pressure into the upper bound theorem, the work rate equation obtained by equating the external work rate to the internal energy dissipation in any kinematically admissible velocity field can be expressed as

$$\int_\Omega \sigma_{ij}\dot{\varepsilon}_{ij}d\Omega \geq \int_S T_i v_i ds + \int_\Omega X_i v_i d\Omega - \int_S n_i v_i u ds \tag{2}$$

where σ_{ij} and $\dot{\varepsilon}_{ij}$ represent the stress tensor and strain rate in the kinematically admissible velocity field respectively; T_i and X_i denote the surface force applied on the boundary S and the body force on the volume of the failure block Ω respectively, v_i corresponds to the detaching velocity along the yield surface, u is the pore water pressure, n_i is the outward unit vector perpendicular to the boundary S (Qin and Chian 2017, Li and Yang 2019a, b, c, Ganesh *et al.* 2018).

2.2 The modified Hoek-Brown failure criterion

The linear Mohr-Coulomb failure criterion is often used to represent the failure curve of soils or rock masses in previous works. However, a good deal of geotechnical experiments show that the friction angle of geomaterials decreases with the increase of confining pressures which eventually leads to a nonlinear failure envelope (Benahmed *et al.* 2017, Li and Yang 2018a). In order to address this problem, Hoek and Brown (1980) proposed the nonlinear failure criterion in an attempt to provide a more reliable way to describe the stress-strain relationship for rock failure, namely the original Hoek-Brown failure criterion. Subsequently, Hoek *et al.* (2002) gave the form of modified Hoek-Brown failure criterion as follows.

$$\sigma_1 = \sigma_3 + \sigma_c\left(m_b\frac{\sigma_3}{\sigma_c} + s\right)^n \tag{3}$$

where σ_1 and σ_3 are maximum and minimum principal stresses respectively; and σ_c is the uniaxial compressive strength of rock. The expressions of m_b, s and n are

$$m_b = m_i \exp\left(\frac{GSI-100}{28-14D}\right) \tag{4}$$

$$s = \exp\left(\frac{GSI-100}{9-3D}\right) \tag{5}$$

$$n = \frac{1}{2} + \frac{1}{6}\left[\exp\left(-\frac{GSI}{15}\right) - \exp\left(-\frac{20}{3}\right)\right] \tag{6}$$

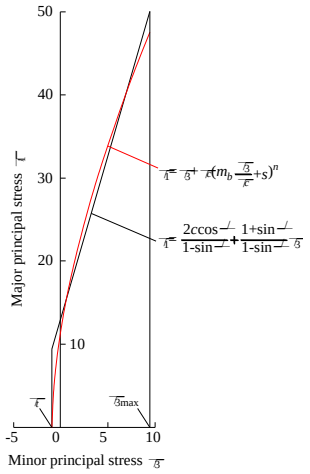

Fig. 1 Redrawing of the relationships between major and minor principal stresses for Hoek-Brown and Mohr-Coulomb failure criteria (Hoek *et al.* 2002)

where m_i represents the rock material constant determined by the rock type; *GSI* is the geological strength index, which represents the integrity of the rock masses; *D* is the disturbance coefficient which varies from 0 for undisturbed rock masses to 1.0 for heavily disturbed ones.

2.3 The equivalent shear strength parameters

Fig. 1 presents the relationships between major and minor principal stresses for Howk-Brown and Mohr-Coulomb failure criteria. It is given by Hoek *et al.* (2002) to fulfill the demand of determining the equivalent cohesion and internal friction angle of Hoek-Brown rock masses in engineering design. As shown in Fig. 1, the equivalent shear strength parameters are obtained based on the principle of balancing the areas above and below the Mohr-Coulomb curve when the minor principle stress ranges from σ_t to σ_{3max}, where σ_t presents the uniaxial tensile strength and σ_{3max} is determined by specified geotechnical engineering problems. Hoek *et al.* (2002) suggested that σ_{3max} can be estimated by the following equation for deep tunnels.

$$\frac{\sigma_{3\max}}{\sigma_{cm}} = 0.47\left[\frac{\sigma_{cm}}{\gamma H}\right]^{-0.94} \tag{7}$$

$$\sigma_{cm} = \sigma_c \frac{\left[m_b + 4s - n\left(m_b - 8s\right)\right]\left(m_b/4 + s\right)^{n-1}}{2\left(1+n\right)\left(2+n\right)} \tag{8}$$

where γ is the unit weight of the rock masses and *H* is the buried depth of the tunnel. Accordingly, the equivalent cohesion *c* and internal friction angle φ are expressed as follows.

$$c = \frac{\sigma_c\left[\left(1+2n\right)s + \left(1-n\right)m_b\sigma_{3n}\right]\left(s + m_b\sigma_{3n}\right)^{n-1}}{\left(1+n\right)\left(2+n\right)\sqrt{1+\left[6m_b n\left(s+m_b\sigma_{3n}\right)^{n-1}\right]\Big/\left(\left(1+n\right)\left(2+n\right)\right)}} \tag{9}$$

$$\varphi = \arcsin\left[\frac{6m_b n\left(s+m_b\sigma_{3n}\right)^{n-1}}{2\left(1+n\right)\left(2+n\right)+6m_b n\left(s+m_b\sigma_{3n}\right)^{n-1}}\right] \tag{10}$$

where $\sigma_{3n}=\sigma_{3max}/\sigma_c$.

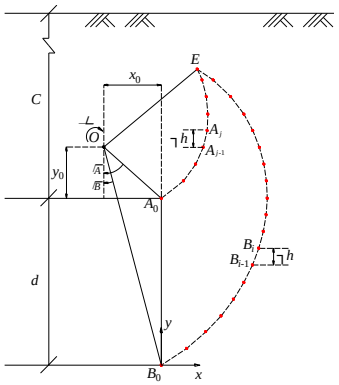

Fig. 2 The schematic of the horizontally layered discretization technique

3. Limit analysis with the horizontally layered discretization technique

3.1 The horizontally layered discretization technique

In most rock tunnel stability analysis, the rock masses are considered as uniform geomaterials with constant rock parameters. However, natural rock deposition usually exhibits depth-dependent properties due to consolidation pressure, stress history and other external factors. To solve this problem, the horizontally layered discretization technique is proposed to perform the kinematical stability analysis of tunnel face. The basic idea of the proposed discretization technique is to find the new points based on the already known points layer by layer and eventually outline the failure domain of tunnel face. This approach has advantage of handling stability problems involving depth-dependent rock parameters.

The proposed approach can be graphically presented in Fig. 2 where *C* represents the buried depth, *d* refers to the diameter of the tunnel, *O* is the rotation center, ω is the angular velocity and θ_A, θ_B respectively denote the rotation angles of OA_0, OB_0. Firstly, the Cartesian coordinate system is built with its origin at point B_0, so the coordinates of B_0 and *O* can be written as $O=(-x_0, y_0+d)$ and $B_0=(0, d)$. Based on the geometric relationship, x_0, y_0 can be expressed in the form of θ_A and θ_B.

$$\begin{cases}\theta_A = \arctan\left(\dfrac{x_0}{y_0}\right)\\ \theta_B = \arctan\left(\dfrac{x_0}{y_0+d}\right)\end{cases} \Rightarrow \begin{cases}x_0 = \dfrac{d\tan\theta_A\tan\theta_B}{\tan\theta_A - \tan\theta_B}\\ y_0 = \dfrac{d\tan\theta_B}{\tan\theta_A - \tan\theta_B}\end{cases} \tag{11}$$

The next step is to generate the new points with respect to the following principles:

- Rotational failure mechanism. The velocity direction of each element should be perpendicular to its rotation radius;
- Associated flow rule. The slipping surface at each point should form an angle of φ with its velocity direction where φ denotes the equivalent internal friction angle of the Hoek-Brown rock masses;
- The principle of equal height. The vertical distance between any two adjacent points is equal to Δh.

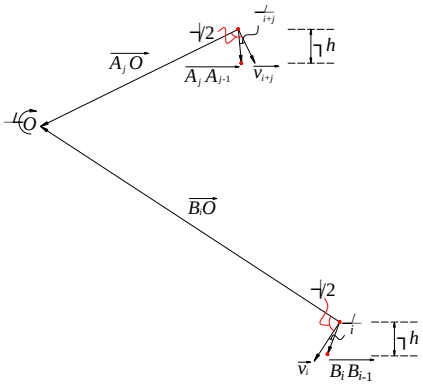

Fig. 3 The vector diagram of geometric relationship for generation of A_j and B_i

The generation of the discretized points are started from A_0 and B_0, which respectively form the upper and lower boundaries of the failure block of tunnel face. According to the principles, the vector diagram of geometric relationship for generation of next points A_j and B_i can be plotted in Fig. 3 where φ_i refers to the equivalent internal friction angle of the i-th element. The vectors listed in Fig. 3 can be represented by coordinates, namely

$$\begin{cases} \overrightarrow{A_jA_{j-1}} = \left(x_{Aj-1} - x_{Aj}, -\Delta h\right) \\ \overrightarrow{A_jO} = \left(-x_0 - x_{Aj}, y_0 + d - (i+j)\Delta h\right) \\ \overrightarrow{B_iB_{i-1}} = \left(x_{Bi-1} - x_{Bi}, -\Delta h\right) \\ \overrightarrow{B_iO} = \left(-x_0 - x_{Bi}, y_0 + d - i\Delta h\right) \end{cases} \tag{12}$$

where i and j are positive integers.

According to the angle relationship of these vectors, the following equation can be obtained.

$$\begin{cases} \cos\left(\pi/2 - \varphi_{i+j}\right) = \dfrac{\overrightarrow{A_jA_{j-1}} \cdot \overrightarrow{A_jO}}{\left|\overrightarrow{A_jA_{j-1}}\right| \cdot \left|\overrightarrow{A_jO}\right|} = \dfrac{x_{Aj}^2 + x_{Aj}\left(x_0 - x_{Aj-1}\right) - x_0 x_{Aj-1} + (i+j)\Delta h^2 - \Delta h\left(y_0 + d\right)}{\sqrt{\left(x_{Aj} - x_{Aj-1}\right)^2 + \Delta h^2}\sqrt{\left(x_{Aj} + x_0\right)^2 + \left[(i+j)\Delta h - y_0 - d\right]^2}} \\ \cos\left(\pi/2 + \varphi_i\right) = \dfrac{\overrightarrow{B_iB_{i-1}} \cdot \overrightarrow{B_iO}}{\left|\overrightarrow{B_iB_{i-1}}\right| \cdot \left|\overrightarrow{B_iO}\right|} = \dfrac{x_{Bi}^2 + x_{Bi}\left(x_0 - x_{Bi-1}\right) - x_0 x_{Bi-1} + i\Delta h^2 - \Delta h\left(y_0 + d\right)}{\sqrt{\left(x_{Bi} - x_{Bi-1}\right)^2 + \Delta h^2}\sqrt{\left(x_{Bi} + x_0\right)^2 + \left(i\Delta h - y_0 - d\right)^2}} \end{cases} \tag{13}$$

Each new point can be determined using Eq. (13). The discretization procedure is continuously run until the condition of $x_{Aj} > x_{Bi+j}$ is satisfied.

3.2 Work rate calculation

According to the horizontally layered discretization technique, the failure block of tunnel face is composed of numerous trapezoidal elements with a same height of Δh, and there is no relative movement between them. So the work rate done by the whole block can be calculated by summing up all the elementary work rate. As shown in Fig. 4, the elementary work rate done by gravity can be expressed as

$$\begin{aligned} P_\gamma' &= \omega\left|\overrightarrow{OM_i}\right|\gamma G_i \cos\left(\frac{\pi}{2} - \theta_i\right) \\ &= \omega\gamma G_i\left(x_{Mi} + x_0\right) \end{aligned} \tag{14}$$

where M_i represents the center of gravity of the i-th element; θ_i denotes the rotation angle of OM_i; γ is the unit

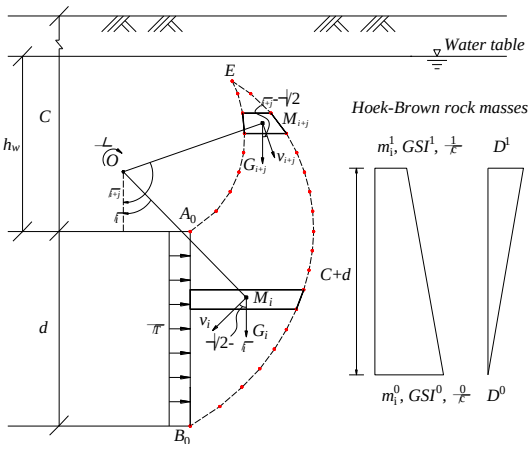

Fig. 4 The work rate analysis of tunnels in Hoek-Brown rock masses considering depth-dependent rock parameters

weight of rock masses; G_i refers to the trapezoidal area. So the work rate of the whole block done by gravity can be calculated as

$$P_\gamma = \omega\sum_{i=1}^{k_1}\gamma G_i\left(x_{Mi} + x_0\right) \tag{15}$$

where k_1 refers to the number of the discretized elements.

For an arbitrary trapezoid whose four vertexes coordinates are known, the trapezoidal area G_i and the x-axis coordinate of its center of gravity x_{Mi+j} can be solved using the following equations.

$$G_i = \frac{1}{2}\Delta h\left(x_{Bi+j} + x_{Bi+j-1} - x_{Aj} - x_{Aj-1}\right) \tag{16}$$

$$x_{Mi+j} = \frac{\left[x_{Bi+j} - x_{Aj} + 2\left(x_{Bi+j-1} - x_{Aj-1}\right)\right]\left(x_{Aj-1} + x_{Bi+j-1} - x_{Aj} - x_{Bi+j}\right)}{6\left(x_{Bi+j} + x_{Bi+j-1} - x_{Aj} - x_{Aj-1}\right)} + \frac{x_{Aj} + x_{Bi+j}}{2} \tag{17}$$

Notice that the elements below the tunnel roof are right-angled trapezoids with x_A=0.

The second part of external work rate is generated by the support pressure applied on tunnel face. As shown in Fig. 4, the acting points of uniform support pressure σ_T are joined in a straight line, so the work rate can be calculated by means of integral.

$$\begin{aligned} P_T &= \int_{\theta_B}^{\theta_A}\sigma_T\frac{\left|\overrightarrow{OB_0}\right|\sin\theta_B}{\sin^2\theta}\omega\frac{\left|\overrightarrow{OB_0}\right|\sin\theta_B}{\sin\theta}\cos\theta d\theta \\ &= \frac{1}{2}\omega\sigma_T\left[x_0^2 + \left(y_0 + d\right)^2\right]\left(1 - \frac{\sin^2\theta_B}{\sin^2\theta_A}\right) \end{aligned} \tag{18}$$

For tunnels excavated under water table whose elevation is denoted as h_w as shown in Fig. 4, the face stability is greatly affected by pore water pressure. In the framework of limit analysis, the pore water pressure is usually considered as a surface force applied on failure surface. So the work rate done by pore water pressure P_u can be computed as

$$P_u = \omega\sum_{j=1}^{k_2}u_j\left|\overrightarrow{A_{j-1}A_j}\right|r_j\sin\varphi_j + \omega\sum_{i=1}^{k_1}u_i\left|\overrightarrow{B_{i-1}B_i}\right|r_i\sin\varphi_i \tag{19}$$

where u_i=the pore water pressure applied on the i-th element, k_2=k_1-$d/\Delta h$ and

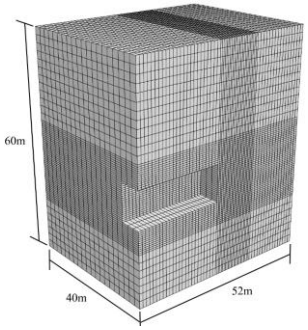

Fig. 5 The numerical model for pore water pressure calculation

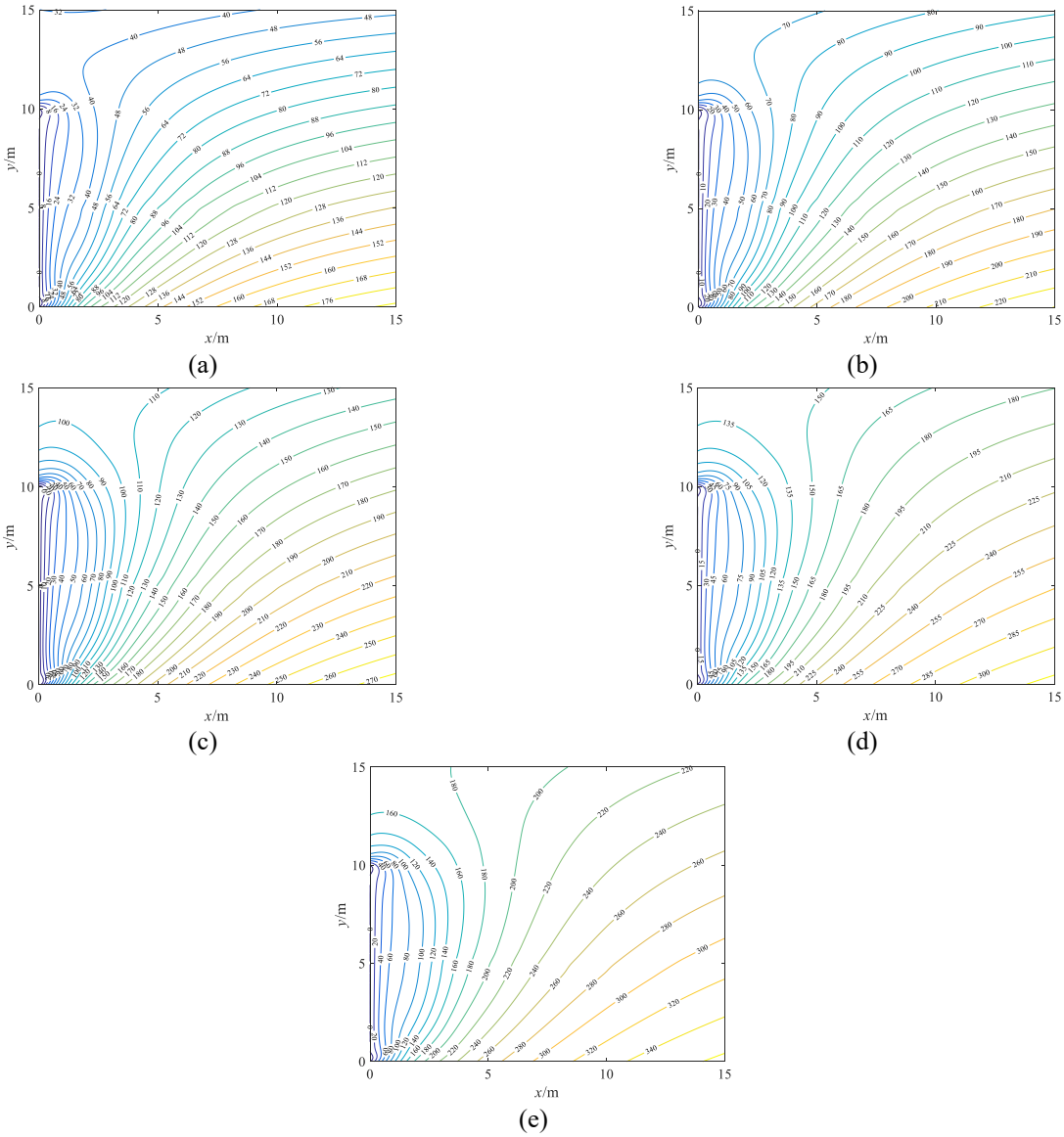

Fig. 6 The pore water pressure distributions ahead of tunnel face (a) h_w=10 m, (b) h_w=15 m, (c) h_w=20 m, (d) h_w=25 m and (e) h_w=30 m

$$\begin{cases} r_i = \sqrt{\left(\dfrac{x_{Bi-1}+x_{Bi}}{2}+x_0\right)^2+\left(\dfrac{y_{Bi-1}+y_{Bi}}{2}-y_0-d\right)^2} \\ r_j = \sqrt{\left(\dfrac{x_{Aj-1}+x_{Aj}}{2}+x_0\right)^2+\left(\dfrac{y_{Aj-1}+y_{Aj}}{2}-y_0-d\right)^2} \end{cases} \tag{20}$$

Based on the assumption of rigid failure block, the energy dissipation P_D is only produced along the sliding surface which is composed of numerous discretized straight lines $\overrightarrow{A_{j-1}A_j}$ and $\overrightarrow{B_{i-1}B_i}$. Accordingly, P_D can be solved as

$$P_D = \omega\sum_{j=1}^{k_2} c_j \left|\overrightarrow{A_{j-1}A_j}\right| r_j \cos\varphi_j + \omega\sum_{i=1}^{k_1} c_i \left|\overrightarrow{B_{i-1}B_i}\right| r_i \cos\varphi_i \tag{21}$$

where c_i and φ_i are the equivalent cohesion and internal friction angle of the i-th element, which are determined by the depth-dependent rock parameters of m_i, GSI, D and σ_c. As shown in Fig. 4, the Hoek-Brown parameters of the rock masses linearly change form m_i^0, GSI^0, D^0 and σ_c^0 at the tunnel invert to m_i^1, GSI^1, D^1 and σ_c^1 at the surface.

According to the upper bound theorem of limit analysis, the upper bound solution of support pressure against face failure can be solved by equating the external work rate to the internal energy dissipation. So the critical support pressure can be obtained by maximizing the objective function of Eq. (22) under the constraint conditions of Eq. (23).

$$\sigma_T = \max\left[\sigma_T \mid P_D = P_\gamma + P_u - P_T\right] \tag{22}$$

$$s.t.\begin{cases} 0 < \theta_B < \dfrac{\pi}{2} \\ \theta_B < \theta_A < \dfrac{\pi}{2} \end{cases} \tag{23}$$

4. Numerical results and discussions

4.1 Pore water pressure calculation

The pore water pressure distribution in front of tunnel face is very irregular for a drained work face. In order to present a more convincing computation, the pore water pressure is numerically calculated by means of 3D steady-state flow analyses using the numerical model given in Fig. 5. The tunnel is assumed as a rectangular one with the diameter d=10 m and buried depth C=30 m, which is composed of 80640 zones and 87360 nodes. The pore water pressures at the symmetry plane of the tunnel are extracted and recorded for each node of the numerical model. In combination with the proposed discretization technique, the pore water pressure for each discretized point is calculated by interpolation based on the extracted data. Fig. 6 presents the contours of pore water pressure in front of tunnel face considering the effects of seepage. The water table elevations of 10 m, 15 m, 20 m, 25 m and 30 m are investigated respectively. It is observed that the pore water pressure at tunnel face is constantly equal to 0 and increases as it moves away from tunnel face and the pore water pressure shows a sharper growth with a higher water table elevation.

4.2 The depth-dependent Hoek-Brown rock masses

This section focuses on tunnel face stability under water table where a more convincing case that the parameters of fractured Hoek-Brown rock masses, namely m_i, GSI, D and σ_c, vary with depth is taken into account. As shown in Fig. 4, m_i, GSI and σ_c increase with depth, while D is on the contrary. For the fractured rock masses, m_i^0, GSI^0, D^0 and σ_c^0 are basically set to 15, 30, 0 and 1.5kPa respectively. The different values of m_i^1, GSI^1, D^1 and σ_c^1 are considered to study their influences on the critical support pressures using the horizontally layered discretization procedure in which the layer height Δh is equal to 0.1 m. The unit weight of dry rock masses γ is set to 22 kN/m^3 and the ratio of saturated rock masses γ_{sat} to γ is set to 1.1 considering the fact that part of the failure block may be above the water table elevation. Fig. 7 presents the equivalent shear strength parameters along the vertical direction considering the poorest Hoek-Brown rock masses with m_i^1=6, GSI^1=5, D^1=1, σ_c^1=0.6 kPa. Table 1 lists the numerical results of critical support pressures with different parameters. It is shown that the effect of pore water pressure on the critical support pressure is remarkable. With the water table elevation ranging from 10 m to 30 m, the critical support pressure varies from 20.05 kPa to 121.19 kPa. Except the pore water pressure, the parameter of GSI^1 have the most

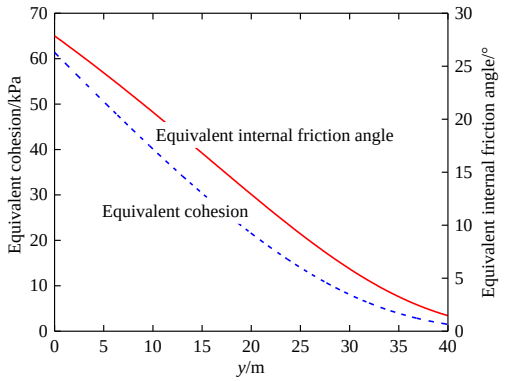

Fig. 7 The equivalent shear strength parameters of Hoek-Brown rock masses with m_i^1=6, GSI^1=5, D^1=1, σ_c^1=0.6 kPa

Table 1 The critical support pressures (kPa) with different parameters

No.	m_i^1	GSI^1	D^1	σ_c^1/kPa	h_w/m	σ_T/kPa
1	15	5	1	0.6	20	63.14
2	12	5	1	0.6	20	64.10
3	9	5	1	0.6	20	64.93
4	6	5	1	0.6	20	66.57
5	6	30	1	0.6	20	59.08
6	6	20	1	0.6	20	60.85
7	6	10	1	0.6	20	64.13
8	6	5	1	0.6	20	66.57
9	6	5	0	0.6	20	62.49
10	6	5	0.4	0.6	20	62.53
11	6	5	0.8	0.6	20	64.15
12	6	5	1	0.6	20	66.57
13	6	5	1	1.5	20	62.48
14	6	5	1	1.2	20	63.64
15	6	5	1	0.9	20	65.02
16	6	5	1	0.6	20	66.57
17	6	5	1	0.6	10	20.05
18	6	5	1	0.6	15	43.64
19	6	5	1	0.6	20	66.57
20	6	5	1	0.6	25	95.36
21	6	5	1	0.6	30	121.19

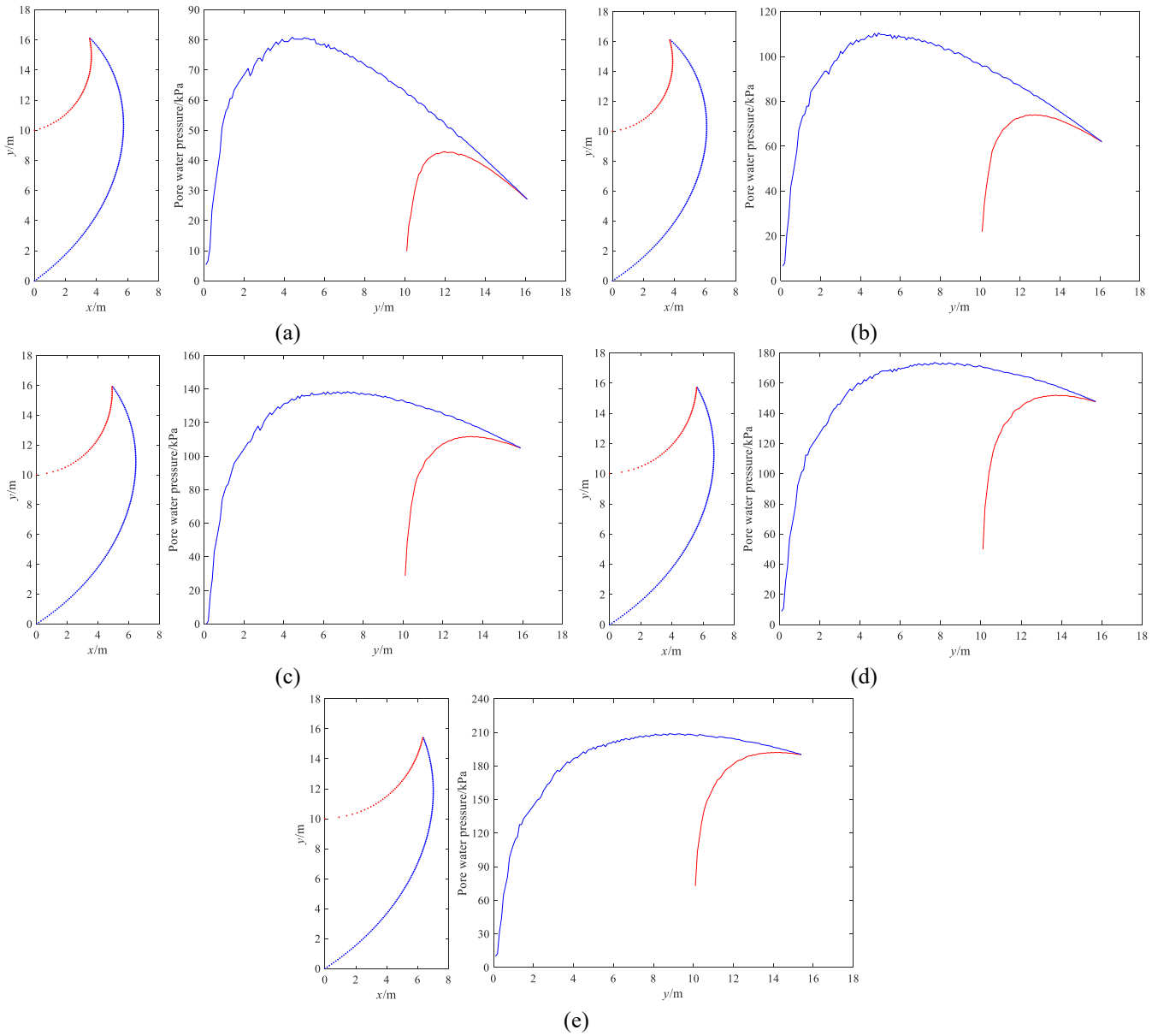

Fig. 8 The failure surface of tunnel face and the corresponding pore water pressures along the upper and lower boundaries for cases in Table 1 (a) No. 17, (b) No. 18, (c) No. 19, (d) No. 20 and (e) No.21

significant influence on tunnel face stability, which results in a range of the critical support pressure from 59.08 kPa to 66.57 kPa.

The extracted pore water pressures are distributed in the whole space ahead of tunnel face, but only the ones applied on failure surface contribute to tunnel collapse. In order to give a more detailed investigation on seepage effects, the pore water pressures along the failure surface are recorded according to the position of the discretized points and plotted in Fig. 8 with respect to the cases from No. 17 to No. 21 in Table 1. The pore water pressures represented by red lines are for the upper boundary and the blue lines for the lower boundary of the failure surface. It can be found that the failure block of tunnel face leans backwards and get lower with the increase of the water table elevation. Totally speaking, the pore water pressure has effects on the shape of failure block and leads to a significant increase of the critical support pressure. In addition, the pore water pressure distributed along the failure surface shows a tendency of firstly increasing and then reducing. This tendency becomes less prominent with the increase of the water table elevation.

4.3 Design charts

According to the numerical results listed in Table 1, the depth-dependent parameters of m_i, GSI, D and σ_c have influence on the critical support pressure, while the variation of water level elevation has the most significant influence. For practical use, several design charts of an undisturbed tunnel with C=30 m and d=10 m are provided in Fig. 9-12, which respectively corresponds to h_w/d=1.5, 2.0, 2.5 and 3.0, for quick evaluations of tunnel face stability. For the case of h_w/d=1.0, the critical support pressure is quite small, so it is not presented in the design charts. The rock parameters at tunnel invert are set as

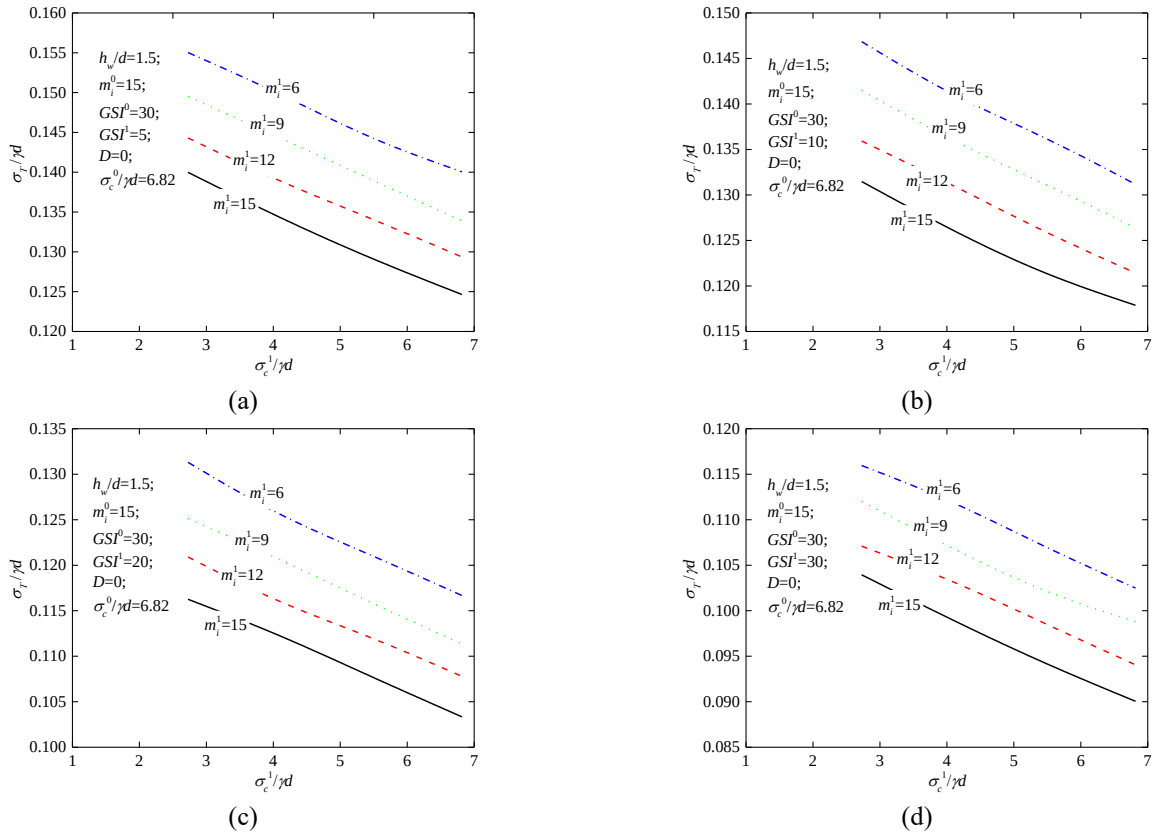

Fig. 9 The normalized critical support pressure versus normalized uniaxial compressive strength at surface with h_w/d=1.5 (a) GSI^1=5, (b) GSI^1=10, (c) GSI^1=20 and (d) GSI^1=30

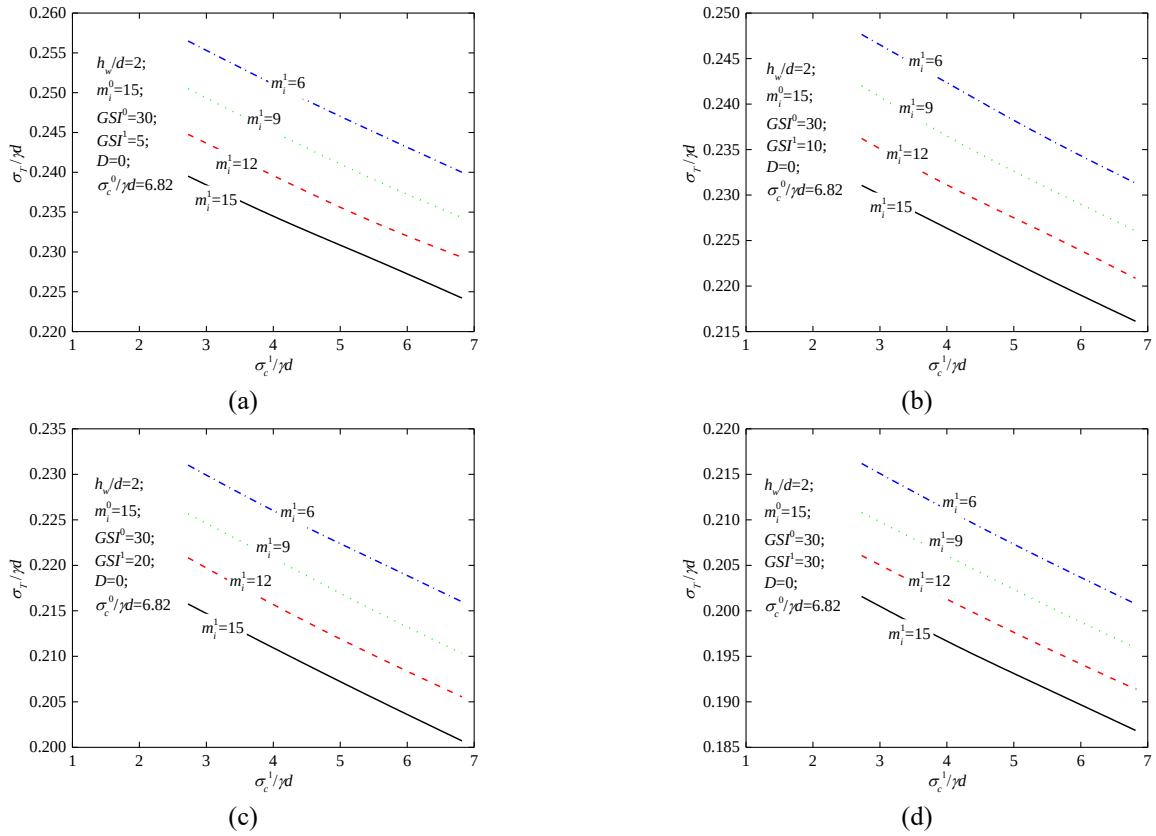

Fig. 10 The normalized critical support pressure versus normalized uniaxial compressive strength at surface with h_w/d=2 (a) GSI^1=5, (b) GSI^1=10, (c) GSI^1=20 and (d) GSI^1=30

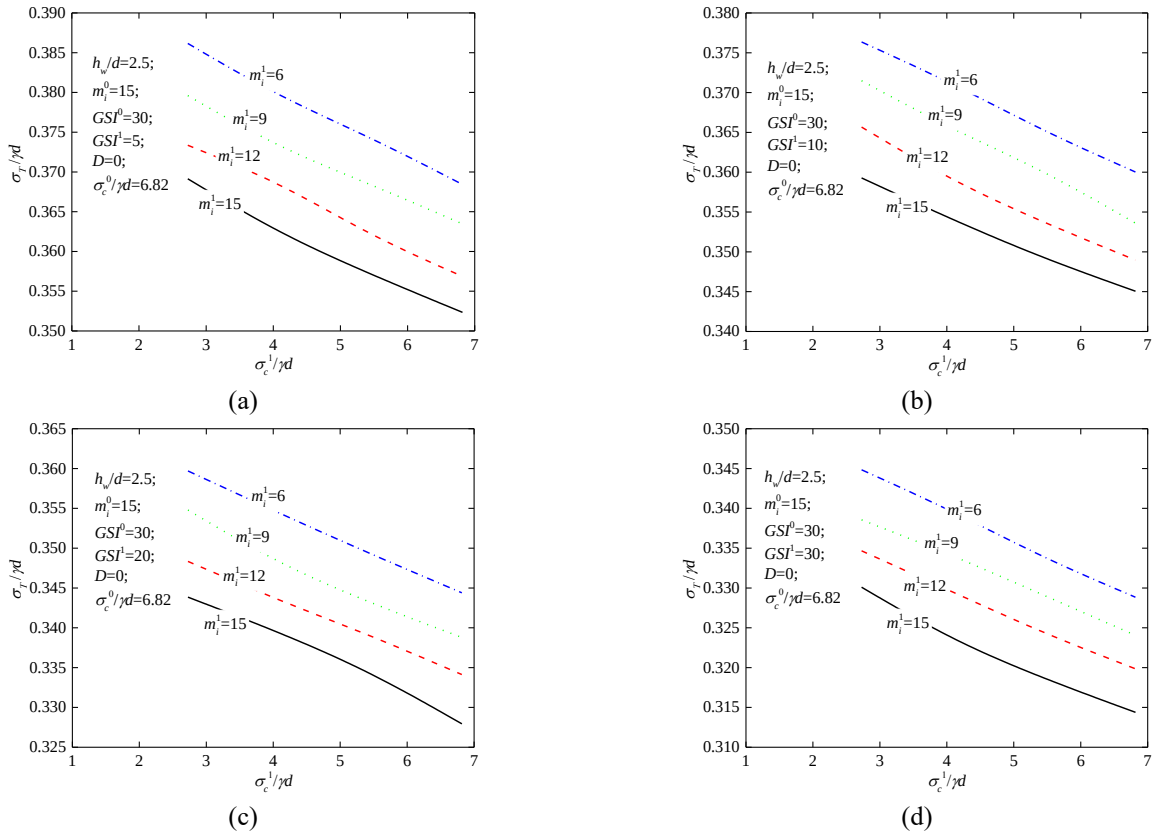

Fig. 11 The normalized critical support pressure versus normalized uniaxial compressive strength at surface with h_w/d=2.5 (a) GSI^1=5, (b) GSI^1=10, (c) GSI^1=20 and (d) GSI^1=30

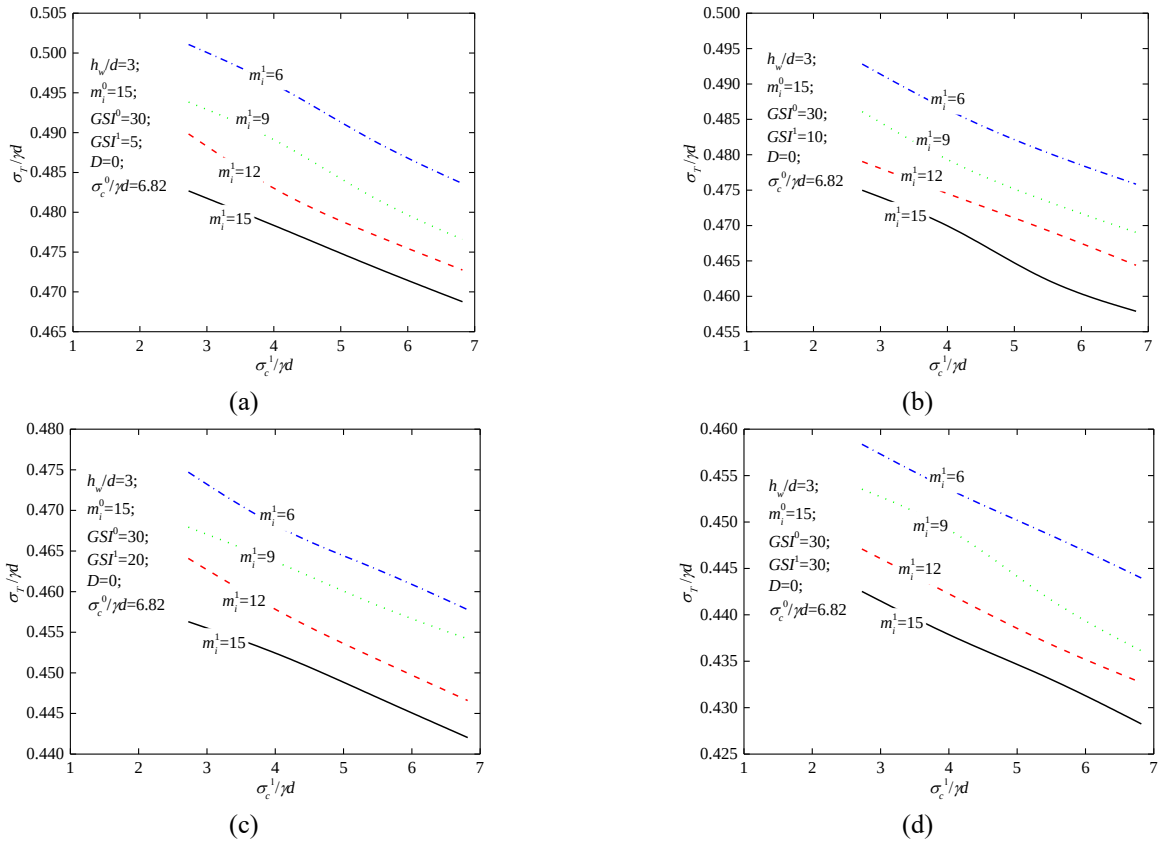

Fig. 12 The normalized critical support pressure versus normalized uniaxial compressive strength at surface with h_w/d=3 (a) GSI^1=5, (b) GSI^1=10, (c) GSI^1=20 and (d) GSI^1=30

m_i^0=15, GSI^0=30, σ_c^0=1.5 MPa. D is set to 0 in all calculations. In the design charts, the normalized critical support pressure $\sigma_T/\gamma d$ is plotted as a function of the normalized uniaxial compressive strength of rock masses at surface $\sigma_c^1/\gamma d$. In each set of figures, GSI^1 changes from 5 to 30 and m_i^1 from 6 to 15. The unit weight of dry rock masses γ is set to 22 kN/m^3 and the ratio of the unit weight of saturated rock masses γ_{sat} to γ is set to 1.1.

As shown in Fig. 9-12, the increase of each parameter of m_i^1, GSI^1, $\sigma_c^1/\gamma d$ leads to the decrease of the normalized critical support pressure. The change curves is nearly linear except a few points that deviated from the straight line. This phenomenon is probably due to the variation of failure surface induced by the depth-dependent rock parameters and the pore water pressure on the failure surface is irregular from a local point of view. The critical support pressure can be directly computed according to the design charts. Thanks to the linear relationship, the critical support pressures for other values of m_i^1, GSI^1, $\sigma_c^1/\gamma d$ can be calculated by linear interpolation.

5. Conclusions

This paper aims to present a procedure to assess the face stability of rock tunnels under water table in the framework of limit analysis using nonlinear Hoek-Brown failure criterion. In order to investigate the influence of depth-dependent rock parameters of m_i, GSI, D and σ_c on face stability, the horizontally layered discretization technique is proposed to generate the failure surface of tunnel face with respect to the three principles mentioned above. To give a better estimation of seepage effect on tunnel face stability, the pore water pressure is numerically computed with resort to the 3D steady-state flow analyses. The data involving the pore water pressure in front of tunnel face are discretely extracted and selected according to the discretized points on failure surface. The upper bound solution of critical support pressure against face failure is calculated by equating the external work rate to the internal energy dissipation. Finally, several design charts are provided for quick calculations of critical support pressures considering an undisturbed tunnel based on the proposed approach.

According to the numerical results, the face stability is greatly affected by the variation of water table elevation. The increase of pore water pressure leads to a wider but lower failure block of tunnel face. Researches on the pore water pressure distributed along the failure surface show that the pressures firstly increase and then decrease along the positive y-axis and this phenomenon becomes less prominent as the increase of water table elevation. With the determined rock parameters at tunnel invert, an increase in m_i^1, GSI^1 and σ_c^1 leads to the decrease of critical support pressure respectively.

The proposed approach is proved to be efficient and accurate in handing stability problems involving depth-dependent rock parameters. The combination of the horizontally layered discretization technique and the discretized pore water pressure data obtained by means of 3D steady-state flow analyses is more convincing in the assessment of tunnel face stability with seepage effects.

Acknowledgments

The preparation of the paper has received financial supports from Innovation Foundation for Postgraduate of Central South University, China (2018zzts185), and National Natural Science Foundation (51378510). The financial supports are greatly appreciated

References

Barros, P.L. and Santos, P.J. (2012), "Coefficients of active earth pressure with seepage effect", *Can. Geotech. J.*, **49**(6), 651-658. https://doi.org/10.1139/t2012-020.

Benahmed, A., Houari, M.S.A., Benyoucef, S., Belakhdar, K. and Tounsi, A. (2017), "A novel quasi-3D hyperbolic shear deformation theory for functionally graded thick rectangular plates on elastic foundation", *Geomech. Eng.*, **12**(1), 9-34. https://doi.org/10.12989/gae.2017.12.1.009.

Bishop, A.W. and Morgenstern, N. (1960), "Stability coefficients for Earth slopes", *Géotechnique*, **10**(4), 129-153. https://doi.org/10.7939/R35M62D9F.

Ganesh, R., Khuntia, S. and Sahoo, J.P. (2018), "Seismic uplift capacity of shallow strip anchors: A new pseudo-dynamic upper bound limit analysis", *Soil Dyn. Earthq. Eng.*, **109**, 69-75. https://doi.org/10.1016/j.soildyn.2018.03.004.

Hamrouni, A., Dias, D. and Sbartai, B. (2018), "Reliability analysis of a mechanically stabilized earth wall using the surface response methodology optimized by a genetic algorithm", *Geomech. Eng.*, **15**(4), 937-945. https://doi.org/10.12989/gae.2018.15.4.937.

Hoek, E. and Brown, E.T. (1980), "Empirical strength criterion for rock masses", *J. Geotech. Geoenviron. Eng.*, **106**(GT9), 1013-1035.

Hoek, E., Carranza-Torres, C. and Corkum, B. (2002), "Hoek-Brown failure criterion-2002 edition", *Proceedings of the 5th North American Rock Mechanics Symposium and the 17th Tunnelling Association of Canada Conference: NARMS-TAC 2002*, Toronto, Canada, July.

Lee, I.M., Nam, S.W. and Ahn, J.H. (2003), "Effect of seepage forces on tunnel face stability", *Can. Geotech. J.*, **40**(2), 342-350. https://doi.org/10.1139/t02-120.

Li, H., Shi, S.L., Lu, J.X., Ye, Q., Lu, Y. and Zhu, X.N. (2019), "Pore structure and multifractal analysis of coal subjected to microwave heating", *Powder Technol.*, **346**, 97-108. https://doi.org/10.1016/j.powtec.2019.02.009.

Li, T.Z. and Yang, X.L. (2019a), "3D rotational failure mechanism of tunnel face in weathered and saturated Hoek-Brown rock masses", *KSCE J. Civ. Eng.*, **23**(6), 2723-2732. https://doi.org/10.1007/s12205-019-1048-4.

Li, Y.X. and Yang, X.L. (2019b), "Seismic displacement of 3D slope reinforced by piles with nonlinear failure criterion", *Int. J. Geomech.*, **19**(6), 04019042. https://doi.org/10.1061/(ASCE)GM.1943-5622.0001411.

Li, Z.W. and Yang, X.L. (2019c), "Active earth pressure from unsaturated soils with different water levels", *Int. J. Geomech.*, **19**(7), 06019013. https://doi.org/10.1061/(ASCE)GM.1943-5622.0001471.

Li, T.Z. and Yang, X.L. (2018a), "Probabilistic stability analysis of subway tunnels combining multiple failure mechanisms and response surface method", *Int. J. Geomech.*, **18**(12), 04018167. https://doi.org/10.1061/(ASCE)GM.1943-5622.0001315.

Li, Z.W. and Yang, X.L. (2018b), "Active earth pressure for soils with tension cracks under steady unsaturated flow conditions", *Can. Geotech. J.*, **55**(12),1850-1859. https://doi.org/10.1139/cgj-2017-0713.

Luo, W.J. and Yang, X.L. (2018), "3D stability of shallow cavity

roof with arbitrary profile under influence of pore water pressure", *Geomech. Eng.*, **16**(6), 569-575. https://doi.org/10.12989/gae.2018.16.6.569.

Michalowski, R.L. (2002), "Stability charts for uniform slopes", *J. Geotech. Geoenviron. Eng.*, **128**(4), 351-355. https://doi.org/10.1061/(ASCE)1090-0241(2002)128:4(351).

Mollon, G., Dias, D. and Soubra, A.H. (2011), "Rotational failure mechanisms for the face stability analysis of tunnels driven by a pressurized shield", *Int. J. Numer. Anal. Meth. Geomech.*, **35**(12), 1363-1388. https://doi.org/10.1002/nag.962.

Mollon, G., Phoon, K.K., Dias, D. and Soubra, A.H. (2010), "Validation of a new 2D failure mechanism for the stability analysis of a pressurized tunnel face in a spatially varying sand", *J. Eng. Mech.*, **137**(1), 8-21. https://doi.org/10.1061/(ASCE)EM.1943-7889.0000196.

Pan, Q. and Dias, D. (2016), "The effect of pore water pressure on tunnel face stability", *Int. J. Numer. Anal. Meth. Geomech.*, **40**(15), 2123-2136. https://doi.org/10.1002/nag.2528.

Pan, Q. and Dias, D. (2018), "Three dimensional face stability of a tunnel in weak rock masses subjected to seepage forces", *Tunn. Undergr. Sp. Technol.*, **71**, 555-566.

Perazzelli, P., Leone, T. and Anagnostou, G. (2014), "Tunnel face stability under seepage flow conditions", *Tunn. Undergr. Sp. Technol.*, **43**, 459-469. https://doi.org/10.1016/j.tust.2014.03.001.

Qin, C. and Chian, S.C. (2017), "2D and 3D stability analysis of tunnel roof collapse in stratified rock: A kinematic approach", *Int. J. Rock Mech. Min. Sci.*, **100**, 269-277. https://doi.org/10.1016/j.ijrmms.2017.10.027.

Skempton, A.W. (1954), "The pore-pressure coefficients A and B", *Géotechnique*, **4**(4), 143-147. https://doi.org/10.1680/geot.1954.4.4.143.

Sloan, S.W. (2013), "Geotechnical stability analysis", *Géotechnique*, **63**(7), 531. http://dx.doi.org/10.1680/geot.12.RL.001.

Ukritchon, B., Yingchaloenkitkhajorn, K. and Keawsawasvong, S. (2017), "Three-dimensional undrained tunnel face stability in clay with a linearly increasing shear strength with depth", *Comput. Geotech.*, **88**, 146-151. https://doi.org/10.1016/j.compgeo.2017.03.013.

Ukritchon, B., Keawsawasvong, S. and Yingchaloenkitkhajorn, K. (2017b), "Undrained face stability of tunnels in Bangkok subsoils", *Int. J. Geotech. Eng.*, **11**(3), 262-277. https://doi.org/10.1080/19386362.2016.1214773.

Ukritchon, B. and Keawsawasvong, S. (2018), "Stability of retained soils behind underground walls with an opening using lower bound limit analysis and second-order cone programming", *Geotech. Geol. Eng.*, **37**(3), 1609-1625.

Ukritchon, B. and Keawsawasvong, S. (2019a), "Stability of unlined square tunnels in Hoek-Brown rock masses based on lower bound analysis", *Comput. Geotech.*, **105**, 249-264. https://doi.org/10.1016/j.compgeo.2018.10.006.

Ukritchon, B. and Keawsawasvong, S. (2019b), "Lower bound stability analysis of plane strain headings in Hoek-Brown rock masses", *Tunn. Undergr. Sp. Technol.*, **84**, 99-112. https://doi.org/10.1016/j.tust.2018.11.002.

Xu, T. and Bezuijen, A. (2018), "Analytical methods in predicting excess pore water pressure in front of slurry shield in saturated sandy ground", *Tunn. Undergr. Sp. Technol.*, **73**, 203-211. https://doi.org/10.1016/j.tust.2017.12.011.

Yang, X.L. and Zhang, R. (2018), "Limit analysis of stability of twin shallow tunnels considering surface settlement", *KSCE J. Civ. Eng.*, **22**(5), 1967-1977. https://doi.org/10.1007/s12205-017-1398-8.

Yang, X.L. and Chen, J.H. (2019), "Factor of safety of geosynthetic-reinforced slope in unsaturated soils", *Int. J. Geomech.*, **19**(6), 04019041. https://doi.org/10.1061/(ASCE)GM.1943-5622.0001399.

Yang, X.L. and Zhang, S. (2019), "Seismic active earth pressure for soils with tension cracks", *Int. J. Geomech.*, **19**(6), 06019009. https://doi.org/10.1061/(ASCE)GM.1943-5622.0001414.

Zhang, D.B., Jiang, Y. and Yang, X.L. (2019), "Estimation of 3D active earth pressure under nonlinear strength condition", *Geomech. Eng.*, **17**(6), 515-525. https://doi.org/10.12989/gae.2019.17.6.515.

Zhang, R. and Yang, X.L. (2019a), "Limit analysis of anchor trapdoor embedded in nonhomogeneous and nonlinear soils", *Int. J. Geomech.*, **19**(8), 04019089. https://doi.org/10.1061/(ASCE)GM.1943-5622.0001476.

Zhang, R. and Yang, X.L. (2019b), "New 3D failure analysis of water-filled karst cave beneath deep tunnel", *Geomech. Eng.*, **18**(1), 1-9. https://doi.org/10.12989/gae.2019.18.1.001.

Zhu, J.Q. and Yang, X.L. (2018), "Probabilistic stability analysis of rock slopes with cracks", *Geomech. Eng.*, **16**(6), 655-667. https://doi.org/10.12989/gae.2018.16.6.655.

CC